Progress In Electromagnetics Research Letters, Vol. 19, 57–65, 2010

MICROWAVE IMAGING BASED ON WIDEBAND RANGE PROFILES

Y. Zhou

Department of Engineering, The University of Texas at Brownsville
80 Fort Brown, Brownsville, TX 78520, USA

Abstract—In this paper, the microwave images of two-dimensional section of multiple objects are formed by using the wideband range profiles of the target. Scattered electric field is obtained by the designed two-dimensional imaging system and Fourier transformed into the highly-resolved range profiles while the target rotates. A filtered back-projection (FBP) algorithm is implemented to form the image from the space domain range profiles. Images of multiple cylindrical rods from both numerically simulated and measured data indicate that the approached imaging scheme can achieve high dynamic range and can be potentially implemented for biomedical imaging detections.

1. INTRODUCTION

Research in microwave imaging involves acquisition of the information (size, shape, location, dielectric properties, other media properties, etc.) for unknown target/media based on the echoed electromagnetic wave. Active microwave imaging has attracted significant interests in biomedical applications (in particular, for breast imaging) since the ultra-wideband (UWB) frequency spectrum (3.1–10.6 GHz) was approved by the FCC in 2002 [1]. With breast cancer becoming the worldwide top killer among all the cancers, microwave imaging for early detection has attracted more research interest to develop and mature it into an alternative detection and screening technique, due to its advantage on cost, safety and noninvasive nature. An important fact that inspires the research on microwave imaging is the 95% survival rate for early detection.

The effectiveness of using microwave for imaging has been investigated in the last decade as alternative to the traditional

Received 6 October 2010, Accepted 16 November 2010, Scheduled 23 November 2010
Corresponding author: Yong Zhou (Yong.Zhou@utb.edu).

X-ray screening and detecting technique. Theoretical study has indicated the feasibility of microwave imaging early detection for breast tumors around 2 mm [2]. Two major approaches are presently under exploration in microwave imaging research: *tomographic methods* where the dielectric properties (dielectric constant, or relative permittivity ε_r) of the imaged area are fully reconstructed, and *radar approach* where strength of the scatterers inside the targeted imaging area are detected and imaged using radar techniques. Tomographic methods (Born and Rytov approximation [3, 4]) are generally based on weak and linear scattering assumptions and usually work well in non-metallic scattering scenarios. Several non-linear numeric iterative schemes [5–10] have been developed to attack the challenges but they are very time-consuming and need further exploration for realistic applications. In recent years, time reversal microwave imaging, which is a new radar-based approach, also attracts much research interest [11]. This approach utilizes the phase-conjugated wave to reduce the distortion due to the heterogeneous media on the propagation path.

In this paper, a microwave imaging scheme is approached and implemented by combining the range profile from radar technique with the tomographic imaging algorithm. Range profile is the one-dimensional signature of the target when the target dimensions are much larger than the wavelength of the incident wave. It can be obtained from the short radar pulse propagating through the target along specific direction, or Fourier transformed from the frequency domain samplings. A microwave tomographic model was developed also by using the chirp radar pulses [12, 13]. It is well known that the resolution of the range profile is inversely proportional to the frequency bandwidth of the incident wave, i.e., $\Delta r = C/2B$, with Δr the spatial resolution, C the speed of light, and B the bandwidth, respectively. When the frequency bandwidth of the microwave signal reaches up to GHz, the obtained range profile can carry the information of the target with centimeter spatial resolution along the wave propagation direction. While the projects of the target are obtained by detecting the penetration density along specific direction in tomography, the range profile can be considered as the projection of the target reflectivity $R(x, y)$ along the direction perpendicular to the incident direction θ, as shown in Fig. 1. When the imaging target rotates, range profiles, or reflectivity projections along discrete directions can be obtained and straightforwardly projected back to the two-dimensional reflectivity map domain. While there are different scan schemes in tomography such as linear scan, fan beam [13] and circular scan, the microwave tomography scheme in this work is similar to the linear scan

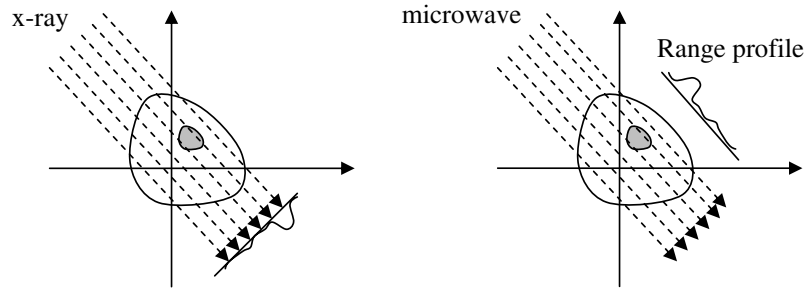

Figure 1. Comparison of x-ray projection and microwave range profile.

scheme.

In practical biomedical UWB imaging applications, special consideration should be taken to reduce the reflection from the skin, which is usually the dominant signal if no reduction scheme is applied [14]. A standard scheme is to immerse the imaging sensors within a matching liquid [15].

The organization of this paper is as follows: Range profile FBP algorithm as well as its implementation in microwave is briefly introduced in Section 2; numerical simulation and comparison with the measured result is detailed in Section 3; the work is finally concluded in Section 4.

2. RANGE PROFILE FBP ALGORITHM AND IMPLEMENTATION

Assume the two dimensional reflectivity map of the imaging region is represented by $R(x, y)$. Continuous Radon transform (RT) of is defined by:

$$\hat{R}(s,\theta) = \iint R(x,y)\delta(s - x\cos\theta - y\sin\theta)dxdy \tag{1}$$

where s and θ are polar coordinates of (x, y) plane, and δ is the unit impulse function. The projection $\hat{R}(s, \theta)$ represents the range profile when incident wave is shooting along the direction θ, with s as the distance from the origin. In this work, only the magnitude of the range profile is used for image reconstruction. It is noticed from the next section that satisfactory image can be obtained even without phase information. Before they are back projected to reconstruct the reflectivity map $R(x, y)$, the projections $\hat{R}(s, \theta)$ are first filtered by the

ramp filter $|s|$:

$$R(x,y) = \int \left[\int \hat{R}(s,\theta) \cdot |s| \cdot \exp[j2\pi(x\cos\theta + y\sin\theta)]ds \right] d\theta$$
$$\cong \sum_{\theta} \left[\int \hat{R}(s,\theta) \cdot |s| \cdot \exp[j2\pi(x\cos\theta + y\sin\theta)]ds\Delta\theta \right] \quad (2)$$

The second line on the above formula is the discrete representation of the integral through θ, as the projection directions are always discontinuous in realistic implementation. It should be noticed that while the ramp filter $|s|$ actually acts as a low pass filter which will significantly depress the low-frequency signal and is necessary for the successful back-projection, it also amplifies the high-frequency noise in the reconstructed image. To reduce the negative effect of the ramp filter, a Hamming window is introduced as a low-pass filter to depress the high-frequency noise level, with the sacrifice of image resolution, however. The adopted discrete Hamming window in this work is as follows:

$$H(n) = 0.54 - 0.46\cos\left(2\pi\frac{n}{N}\right), \quad 0 \le n \le N \quad (3)$$

To implement the proposed scheme, an imaging system is setup on a wooden turntable with two X-band (8 to 12 GHz) horn antennas working as the transmitter/receiver. The imaging target is positioned in the central area of the turntable and is supported by the PC-controlled Yaesu G5500 dual-axis step rotator. Step rotator can drive the positioned imaging target to rotate with an accuracy of 1°. A HP E8364B microwave vector network analyzer is utilized for microwave scattering data acquisition. The whole microwave imaging system is shown in Fig. 2. Along each direction, the horn antennas sweep the band from 8 to 12 GHz and collect the scattered electric field. A straight fast Fourier transform (FFT) transforms the frequency domain field into the spatial range profile $\hat{R}(s,\theta)$.

ETS-Lindgren 3160 X-band horn antennas are placed around the targeting area as the imaging sensors. These wideband antennas have better performance under the controlled environment like the microwave anechoic chamber, but the measured performance is still satisfactory even with the background noise. Fig. 3 shows the measured S_{11} performance of the antenna in its imaging position. The designed imaging system utilizes the frequency band from 8 to 12 GHz, which will guarantee -15 dB performance across the 4 GHz operating band. The frequencies are sampled every 10 MHz, with 401 samples along each direction. Because of the limited bandwidth of the detection system, theoretically it is impossible to recover all of the available

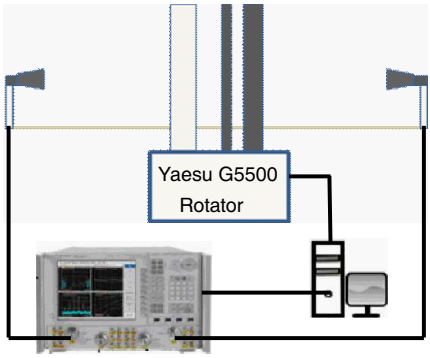

Figure 2. Microwave imaging system.

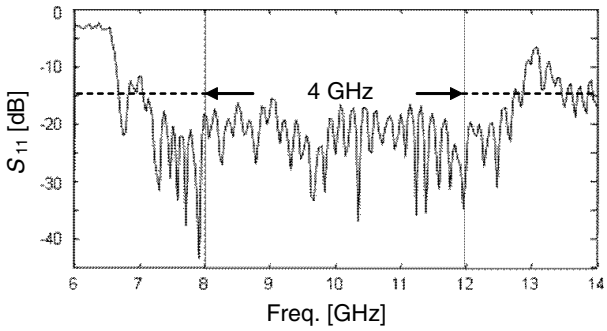

Figure 3. Measured S_{11} of the horn antenna with background noise.

information in the original reflectivity map $R(x, y)$. But 4 GHz bandwidth can still achieve a theoretical 3.75 cm resolution.

3. NUMERICAL RESULTS AND COMPARISON WITH MEASUREMENT

A point scatter is first positioned at the origin to study the resolution of the implemented imaging system. By sweeping the 8–12 GHz spectrum band along the azimuth angle from 0 to 180° by every 2°, the scattered field is simulated and Fourier transformed into the range profiles $\hat{R}(s, \theta)$. The central slice of the resulted image back projected from Eq. (2) indicates the predicted 2.75 cm (at −10 dB) resolution for a 4 GHz bandwidth system, as shown in Fig. 4 (thin line). With the adoption of Hamming window to depress the high-frequency noise level, the resolution is slightly reduced to 4.5 cm at −10 dB, as indicate in Fig. 4 (bold line).

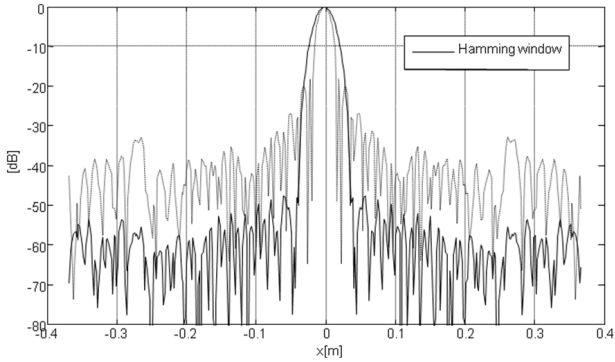

Figure 4. Resolution of imaging system.

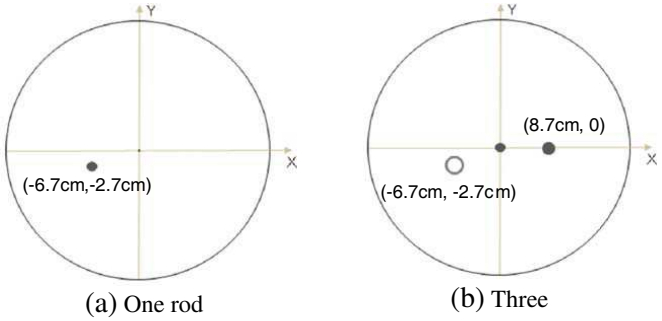

Figure 5. Imaging targets: one and three cylindrical rods.

Two different imaging scenarios are set up to test the imaging algorithm. The first imaging target is a single metallic rod with a radius of 1 cm. The rod is centered at (−6.7 cm, −2.7 cm). The second imaging target is composed of two metallic rods and one PVC rod ($\varepsilon_r = 2.85$, $\delta = 0.00702$). In this case, the radius of the central and the right side metallic rod are 1 cm and 2.1 cm, respectively. The external and internal radius of the hollow PVC pipe is 3.1 cm and 2.1 cm, respectively. The two metallic rods are centered at (0, 0) and (8.7 cm, 0), and the PVC hollow pipe is centered at (−6.7 cm, −2.7 cm). The schematic geometry of the two imaging target configurations is indicated in Fig. 5.

In the first case, the resulted image (Figs. 6(a)) indicates a good correlation of the location and the approximate size of the metallic rod. The slight distortion of the circle-shaped rod in experimental result may be due to the mutual scattering effect among the closely

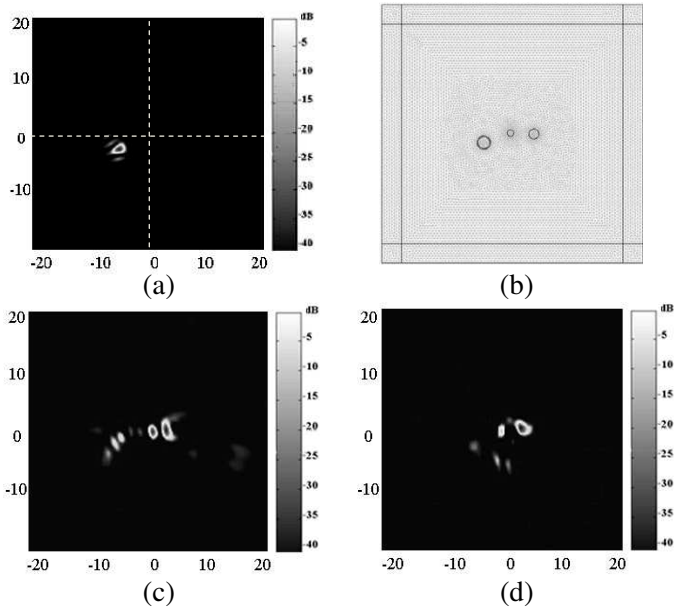

Figure 6. (a) Image formation for single rod. (b) Simulation by COMSOL solver for three rods. (c) Image from simulation for three rods (in cm). (d) Image from measurement for three rods (in cm).

located metallic rods. Another source of the distortion is the fact that the imaging reconstruction algorithm does not take into account the finite size of the horn antenna. It needs extra effort to exactly compensate such effects in the back projection algorithm. In the second case, microwave images of two-dimensional sections of single and multiple objects are first simulated by the finite-element-method-based COMSOL Multiphysics solver. Fig. 6(b) shows the discrete COMSOL model of the imaged targets. The perfectly matched layers (PMLs) are introduced to surround the air domain representing absorbing layers. Figs. 6(c) and (d) show images from COMSOL simulated data and measured data, respectively. It should be noticed that the two metallic rods contribute much stronger scattering than the PVC hollow pipe. Both images in Figs. 6(c) and (d) have shown all the three well resolved rods, indicating a satisfactory dynamic range. The estimated resolution for the resulted image from measurement is around 5 cm, which slightly degenerates from the theoretical one because of the Hamming windows implementation. Still the slight shape distortion of the circle-shaped rods can be observed in both simulated and measured results, as indicated in the single rod case.

4. CONCLUSION

A wideband microwave imaging scheme is implemented and verified by simulated and measured results. The imaging scheme utilizes high-resolution range profiles as projections to reconstructs the target cross sectional reflectivity by filtered back-projection algorithm. Specific details describing the measurement of three cylindrical rods with different dielectric and conductivity as well as the implementation of the reconstruction algorithm are discussed. The reconstructed images from both simulation and measured data correlate well in position with the imaged target. Imaging results also indicate an estimated 5 cm resolution and good dynamic range. However, slight shape distortion can be observed in the resulted images, which may be due to the mutual scattering effect and ignorance of the finite size of the horn antenna in the imaging reconstruction algorithm. Since the dielectric PVC rod has close dielectric properties to some of the human tissues, the implemented scheme can be potentially extended to study its applications in microwave screening and detection.

ACKNOWLEDGMENT

This work was in part supported by Major Research Instrumentation program of National Science Foundation under award No. ECCS-0723113. The author would like to thank Patricia M. Garcia for her help on imaging system setup and data acquisition.

REFERENCES

1. Federal Communications Commission Report FCC 02-48, 2002.
2. Xie, Y., B. Guo, L. Xu, L. Jian, and P. Stoica, "Multistatic adaptive microwave imaging for early breast cancer detection," *IEEE Trans. Biomed. Eng.*, Vol. 53, No. 8, 1647–1657, Aug. 2006.
3. Slaney, M., A. C. Kak, and L. E. Larsen, "Limitations of imaging with first-order diffraction tomography," *IEEE Trans. Microwave Theory Tech.*, Vol. 32, 860–874, Aug. 1984.
4. Joisel, A. and J.-C. Bolomey, "Rapid microwave imaging of living tissues," *SPIE Symp. Medical Imag.*, San Diego, CA, USA, Feb. 12–18, 2000.
5. Jofre, L., M. S. Hawley, A. Broquetas, E. de Los Reyes, M. Ferrando, and A. R. Elias-Fuste, "Medical imaging with a microwave tomographic scanner," *IEEE Trans. Biomed. Eng.*, Vol. 37, 303–311, Mar. 1990.
6. Bolomey, J.-C., A. Izadnegahdar, L. Jofre, C. Pichot, G. Peronnet,

and M. Solaimani, "Microwave diffraction tomography for biomedical applications," *IEEE Trans. Microwave Theory Tech.*, Vol. 30, 1998–1982, Nov. 1982.

7. Pichot, C., L. Jofre, G. Peronnet, and J.-C. Bolomey, "Active microwave imaging of inhomogeneous bodies," *IEEE Trans. Antennas Propagat.*, Vol. 33, 416–423, Apr. 1985.
8. Pan, S. X. and A. C. Kak, "A computational study of reconstruction algorithms for diffraction tomography: Interpolation versus filtered backpropagation," *IEEE Transactions on Acoustics, Speech and Signal Processing*, Vol. 31, 1262–1275, Oct. 1983.
9. Caorsi, S., M. Donelli, D. Franceschini, and A. Massa, "An iterative mutiresolution approach for microwave imaging applications," *Microwave and Optical Technology Letters*, Vol. 32, No. 5, Mar. 5, 2002.
10. Winters, D. W., J. D. Shea, P. Kosmas, B. D. van Veen, and S. C. Hagness, "Three dimensional microwave breast imaging: Dispersive dielectric properties estimation using patient-specific basis functions," *IEEE Trans. Med. Imag.*, Vol. 28, No. 7, 969–981, Jul. 2009.
11. Lev-Ari, H. and A. J. Devaney, "The time-reversal technique re-interpreted: Subspace-based signal processing for multi-static target location," *1st IEEE Sensor Array and Multichannel Signal Processing Workshop (SAM'00)*, 509–513, Cambridge, MA, USA, 2000.
12. Miyakawa, M., K. Orikasa, M. Bertero, P. Boccacci, F. Conte, and M. Piana, "Experimental validation of a linear model for data reduction in chirp-pulse microwave CT," *IEEE Transactions on Medical Imaging*, Vol. 21, No. 4, 385–395, 2002.
13. Miyakawa, M., T. Takahashi, N. Iwata, N. Ishii, and M. Bertero, "Fan beam-type CP-MCT with microstrip dipole array receiving antenna," *The 36th European Microwave Conference*, 1244–1247, Sep. 10–15, 2006.
14. Williams, T., E. C. Fear, and D. W. Westwick, "Tissue sensing adaptive radar for breast cancer detection: Investigations of reflections from the skin," *IEEE Antennas and Propagation Society International Symposium*, Vol. 3, 2436–2439, 2004.
15. Fear, E. C. and M. A. Stuchly, "Confocal microwave imaging for breast tumor detection: Comparison of immersion liquids," *IEEE Antennas and Propagation Society International Symposium*, Vol. 1, 250–253, 2001.